Volume 6, Issue 12, December 2016 ISSN: 2277 128X

International Journal of Advanced Research in Computer Science and Software Engineering

Research Paper

Available online at: www.ijarcsse.com

Effect of Doping and Post Annealing on the Structural and Morphological Properties of $Zn_{1-X}Mg_xO$ Nanoparticles Grown by Sol-Gel Method

A. Bendoumou, A. Belahmar, A. Chouiyakh

Department of Physics, Renewable Energy and Environment Laboratory, Faculty of Science, Ibn Tofail University, B.P.133, 14000, Kenitra, Morocco

Abstract— Magnesium-doped ZnO nanoparticles with compositional formula $Zn_{1-x}Mg_xO$ $(where, x = 0.0, 0.02, 0.10, 0.15)$ ***were synthesized by a simple sol–gel method. No diffraction peaks related to the impurities was observed in XRD patterns, indicating the high purity of the synthesized nanopowders. The average crystalline size, strain and lattice parameters of the ZnO nanoparticles are significantly affected by Mg doping and thermal annealing. The surface morphology of the pellets samples was examined by scanning electron microscopy (SEM) approves the nanostructure nature of the ZnO particles, and the EDX confirms the incorporation of Mg in ZnO nanoparticles. All the samples were observed to be nonstoechiometric. The effects of doping and annealing temperature on structural properties are discussed.***

Keywords— Zinc oxide, nanopowders, sol-gel method, SEM, XRD.

I. INTRODUCTION

Zinc oxide is a semiconductor with a wide and a direct band-gap around 3.37eV, which makes its transparency in the visible region of the electromagnetic spectra, and with a large exciton binding energy of 60 meV at room temperature (e.g. [1]). It well known that zinc oxide has been commonly used in its polycrystalline form for a long-time in a wide range of applications, such as sunscreens, catalyst, lubrifiant addition, varistors, etc. Due to its remarkable properties at manometer scale, there has been a special interest in the study of zinc oxide nanostructures both on fundamental and practical scale in the last decades. Numerous papers can be found in the literature giving recent advances on ZnO nanostructures grown by different methods (e.g. [2]-[3]-[4]). In this connection, nanostructured ZnO powders have attracted great interest due to their widely potential applications such as water treatment (e.g. [5]), gas sensors (e.g.[6]), solar cells (e.g.[7]) and thermoluminescence dosimetry (e.g.[8]-[9]). The size of ZnO particles in these powders is a very important factor for the specific applications. Indeed, from technological point of view, fine powders materials offer significant advantage over the crystals due to the ease and low cost of fabrication.

Doping semiconductor nanostructures in order to control their physical properties is an active field of research related to the development of nanotechnology applications. Due to the variety of ZnO applications, nanostructures of this semiconducting oxide have been doped with different metal ions, including transition metal elements (Ni, Fe, Mg, Co, V, etc.) (e. g. [10]-[17]).

Various methods have been adopted for the preparation of ZnO powders, such precipitation method (e.g. [18]), sol gel processing (e.g. [19]) and mechanical milling (e.g. [20]). The sol-gel has some advantages such low temperature synthesis, high purity, homogeneity, repeatability, and particularly its sheapness and simplicity.

In this work, a simple sol gel method was used to prepare ZnO nanoparticles. The effects of Mg content and post annealing on structural, morphological properties of the obtained nanopowders were investigated.

II. EXPERIMENTAL METHODS

2.1. Synthesis method

ZnO particles were prepared by sol–gel method using zinc acetate as the precursor. A 4.4g zinc acetate (Zn $(CH_3COO)_2$, $2H_2O$) (solution A) and 2 g sodium hydroxide (solution B) were dissolved in 100 ml of distilled water and treated in 35 and 20 ml ethanol at 50°C respectively. Solution B was added drop wise with constant stirring to a warm solution of A. This would result in the appearance of turbidity in the solution leading to the formation of ZnO in the form of gel. After the complete addition, the resulting solution was stirred overnight which was then filtered, washed with water and dried at 100◦C for 2h, manually ground and calcined at 200°C for 3h to give pure ZnO. This ZnO was taken as reference.

In order to obtain $ZnO_{1-x}Mg_xO$ nanoparticles, an adequate amount of ($MgSO_4$, $7H_2O$) with Mg / Zn proportions of (0.00, 0.02, 0.10 and 0.15) are dissolved in required amount of ethanol, were added to the solution A along with solution B simultaneously. After stirring the solution over night (ZnO-doped) was formed, which was filtered, washed with distilled water to remove the excess-ions and insoluble materials remaining in the product and dried at 100°C for 2h.

The powdered material obtained was manually ground and calcined at 200°C for 3h. The precursor masses are summarized in Table 1.

Table1. Different proportions in Mg/Zn with the precursors masses.

Proportions x	Mass: (g) of Zn (CH3COO2), 2H2O	Mass: (g) of MgSO4, 7H2O
00	4.4	00
0.02	4.4	0.1
0.1	4.4	0.5
0.15	4.4	1

2.2. Characterization techniques

The structure and crystallite size of Mg-doped ZnO NPs were determine by X-ray diffraction (XRD) using Cu-Kα radiations ($\boldsymbol{\lambda = 0.14506\ nm}$) in $\boldsymbol{2\theta}$ range from $\boldsymbol{10^{\circ}}$ to $\boldsymbol{80^{\circ}}$ and the morphological analysis of the sample was carried out on a Scanning Electron Microscope (SEM) (Model: SH 4000M). The composition analysis was carried out using EDAX attached with the SEM. Fourier transform infrared (FT-IR) spectra of as-prepared samples were recorded using a Fourier transform infrared spectrometer (VERTEX/70/70V) in the range of $\boldsymbol{4000 - 400\ cm^{-1}}$ with a resolution of cm^{-1}.

III. RESULTS AND DISCUSSIONS

In the present work, we report the effect of Mg doping and thermal annealing on the structural and morphological properties of $Zn_{1-x}Mg_xO$ (where $x = 0.0, 0.02, 0.10, 0.15$) by sol-gel method. We study the effect of doping in the first paragraph, while the annealing effect will be studied in the second paragraph.

3.1. Doping effect on structural an morphological properties

3.1.1. Structural properties

3.1.1.1. XRD spectra analysis

The characteristic XRD spectra of the pure and Mg-doped ZnO NPs are shown in Fig. 1. Strongly pronounced peaks, <100>, <002> and <101> appear at 2θ= 31.43°, 34.13° and 35.93° respectively, which indicate that the samples are polycrystalline. The peak positions of each sample exhibit the hexagonal wurtzite structure of ZnO, with a dominant <101> peak around $2\theta = 37.5^{\circ}$, which were confirmed from the (JCPDS 79-2205 card). Further, no diffraction peaks related to the impurities was observed in XRD patterns, when the Mg contents is up to 15%, confirming the high purity of the synthesized nanopowders.

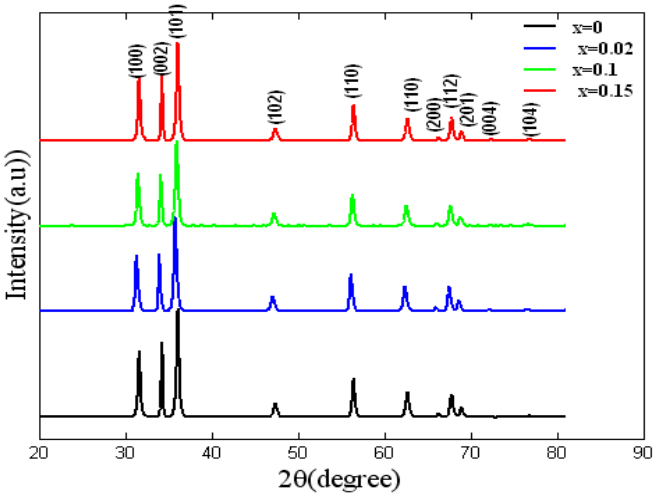

Fig.1. XRD spectra of the un-doped and Mg doped ZnO nanoparticles for different doping contents.

Fig.2 shows the XRD spectra of <100> oriented peaks of $(Zn_{1-x}Mg_xO, x = 0.0, 0.02, 0.10, 0.15)$ nanoparticles and clearly depicts that the sample $Zn_{0.98}Mg_{0.02}O$, shows noticeable peak shifting towards lower 2θ from the standard value. There is not distinguished peak shifting for the sample $Zn_{0.85}Mg_{0.15}O$. From the XRD spectra, the growth of crystals towards <101> orientation was suppressed by higher concentrations of Mg in the ZnO lattice. This result implies that the doping of Mg introduces a certain amount of defects in ZnO host lattice (e.g. [21]).

3.1.1.2. Texture Coefficient Analysis

The quantitative information concerning the preferential crystal orientation can be obtained from the texture coefficient, TC, which can be defined as (e.g. [22]):

$$\boldsymbol{TC_{(hkl)} = \left(\frac{I_{(hlk)}}{I_{0(hkl)}}\right) \Big/ \left[\frac{1}{N}\sum_n \frac{I_{(hlk)}}{I_{0(hkl)}}\right]} \quad \textbf{(1)}$$

where $TC_{(hkl)}$ is the texture coefficient, $I_{(hlk)}$ is the intensity of the XRD of the sample and n is the number of diffraction peaks considered. $I_{0(hkl)}$ is the intensity of the XRD reference of the randomly oriented grains. If $TC_{(hkl)} \approx 1$ for all the $\langle hkl \rangle$ planes are considered, then the nanoparticles are with a randomly oriented crystallite similar to the JCPDS reference, while values higher than 1 indicate the abundance of grains in a given $\langle hkl \rangle$ direction. Values $0 < TC_{(hkl)} < 1$ indicate the lack of grains oriented in that direction. As $TC_{(hkl)}$ increases, the preferential growth of the crystallites in the direction perpendicular to the $\langle hkl \rangle$ plane is greater. In this analysis, three reflections are considered .From the Table 2, the $\langle 002 \rangle$ orientation is the preferred growth in their direction for all Mg content.

Table.2 2θ ,⟨hkl⟩, d_{hkl} ,$strain$,$Lattice\ parametr$,$Particle\ Size$ and $TC_{(hkl)}$ of as deposited $Zn_{1-x}Mg_xO$ samples.

Compound	$2\theta\ value(°)$	⟨hkl⟩	$d_{hkl}(Å)$	*strain* ($\varepsilon \times 10^{-3}$)	*Lattice parametr* ($A°$)	*Particle Size* D_{hkl} (nm)	*Average Size* (nm)	$TC_{(hkl)}$
ZnO	31.6667	⟨100⟩	2.102	4.5	a = 3.2600	28.19758	31.30	1.0417
	34.2916	⟨002⟩	2.271	3.0	c = 5.2258	39.38684		**1.5514**
	36.1396	⟨101⟩	2.389	4.2	c/a = 1.6030	26.3106		0.9495
$Zn_{0.98}Mg_{0.02}O$	31.3708	⟨100⟩	2.083	5.5	a = 3.2900	23.53183	28.07	0.9308
	33.9861	⟨002⟩	2.251	3.2	c = 5.2714	37.30787		**1.3250**
	35.8428	⟨101⟩	2.370	4.8	c/a = 1.6023	23.37395		0.9087
$Zn_{0.9}Mg_{0.1}O$	31.5283	⟨100⟩	2.093	5.7	a = 3.2740	22.51338	24.64	1.0153
	34.1490	⟨002⟩	2.262	3.9	c = 5.2470	29.95887		**1.3511**
	36.0066	⟨101⟩	2.381	5.2	c/a = 1.6026	21.44836		0.9323
$Zn_{0.85}Mg_{0.15}O$	31.6565	⟨100⟩	2.101	4.9	a = 3.2610	26.10515	29.02	1.0612
	34.2476	⟨002⟩	2.270	3.2	c = 5.2280	36.84059		**1.5053**
	36.1317	⟨101⟩	2.389	4.6	c/a = 1.6032	24.12869		0.9348

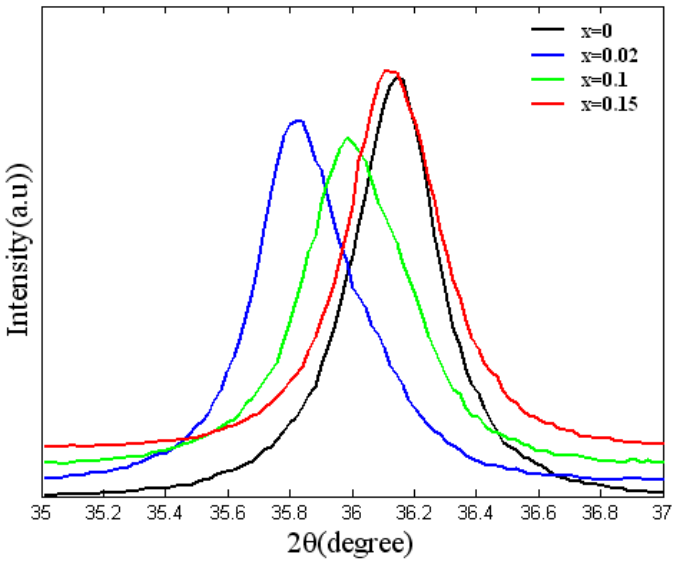

Fig.2. Evolution of the preferred orientation peak <101> with various Mg contents.

3.1.1.3. Crystallite size, Lattice Strain, Dislocation density Stress and Bond Length Analysis.

The crystallite size was estimated for the powder from the full width at half maximum of the diffraction peaks using Scherrer's method and Williamson Hall modified form of uniform deformation model (UDM), uniform stress deformation model (USDM), uniform deformation energy-density model (UDEDM).

3.1.1.3.1. Scherrer method

Te influence of Mg doping on the structural properties can be evaluated by estimating of the lattice constants, crystallite size and strain of the sample from the XRD spectra. Thus, from the Bragg angle position, the crystalline size of the un-doped and Mg doped ZnO nanoparticles were calculated by using the Debye Scherer's formula (e.g. [23]):

$$\mathbf{D = k\lambda/\beta \cos \theta} \qquad \mathbf{(2)}$$

where β is the full width at half maximum (FWHM) of the peaks at the diffracting angle θ. The calculated particle sizes of un-doped and Mg doped samples were obtained in the range of 29.02 nm-31.30 nm as tabulated in Table 2 and plotted in Fig .3. It can be observed from this Figure that the crystallite size of pure ZnO is 31.30 nm which decreases to 24.63 nm in the sample $Zn_{0.9}Mg_{0.1}O$. Increasing in Mg doping content can be increase the of $Zn_{1-x}Mg_xO$ nanoparticles. The similar results about crystallite size and lattice strain have been reported in the case of Al-doped ZnO thin films (e. g [24]), indium-doped ZnO thin films (e.g. [25]) and Mg-doped ZnO thin films (e.g. [26]). The data reveals that the presence of Mg ions in ZnO prevents the growth of crystal grains.

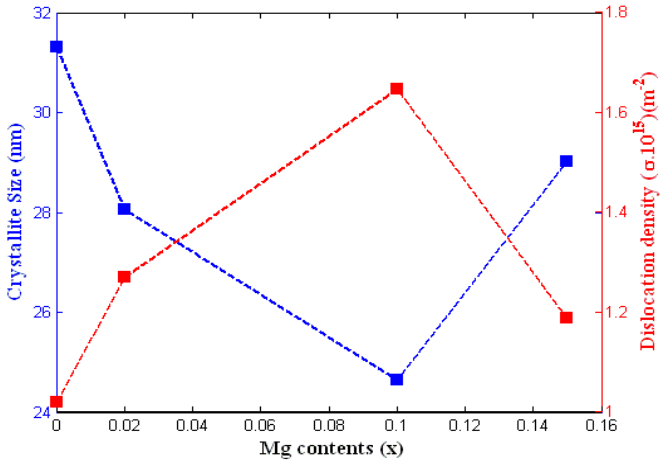

Fig.3 Crystallite size and dislocation density values of the $Zn_{1-x}Mg_xO$ dependence on Mg contents.

The lattice strain (ε) has been determined by using the tangent formula (e. g .27]):

$$\boldsymbol{\varepsilon = \beta/4\tan\theta} \quad \textbf{(3)}$$

The calculated values are listed in Table 2 and plotted in fig.4. It clearly shows that the un-doped sample shows low lattice strain values than as the doped samples. Fig.4 clearly explains the influence of Mg doping on lattice strain with respect to the crystal orientation of un-doped and Mg doped samples. The value of strain increases in all three directions, the maximum value is obtained for $Zn_{0.9}Mg_{0.1}O$. We note that the increase of strain leads to the reduction in the nanoparticles size.

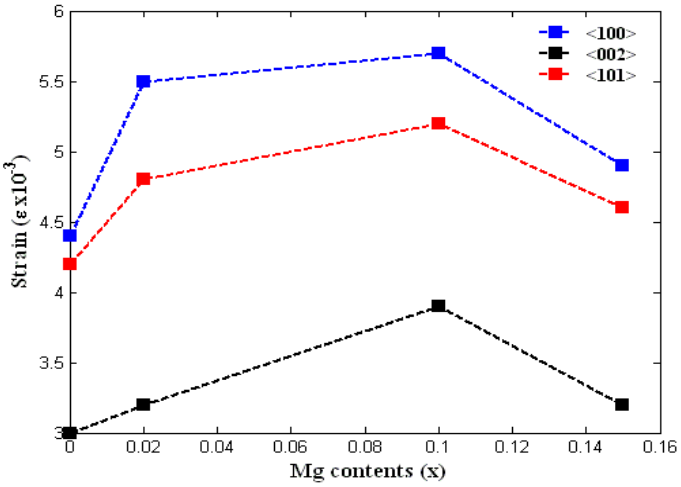

Fig. 4 Strain versus Mg contents of $\mathbf{Zn_{1-x}Mg_xO}$ samples.

To understand the effect of Mg doping on lattice parameters of ZnO, the lattice parameters should be measured for un-doped and Mg doped ZnO nanoparticles. Since ZnO lattice is wurtzite structure with hexagonal shape, there are two lattice parameters *a* and *c* are exist and can be measured by the following relations (e.g. [28]):

$$\boldsymbol{d_{(hkl)} = \left[\frac{4}{3}\left(\frac{h^2+kl+k^2}{a^2}\right)+\frac{l^2}{c^2}\right]^{-1/2}} \quad \textbf{(4)}$$

The lattice constant a for $\langle 100\rangle$ plane is calculated by (e.g.[28]):

$$\boldsymbol{a = \lambda/\sqrt{3}\,Sin\theta} \quad \textbf{(5)}$$

For the $\langle 002\rangle$ plane, the lattice constant c is calculated by (e.g. [28]):

$$\boldsymbol{C = \lambda/Sin\theta} \quad \textbf{(6)}$$

where λ is the X-ray wavelength and $d_{(hkl)}$ is the spacing between planes of given Miller indices h, $k$and l. Using the relation given in equation (4) and (5), the lattice parameters of un-doped and Mg doped ZnO nanoparticles were calculated and the observed results are summarized in Table 2. It is observed that *a* and *c* values varies with Mg content, however $c/a = 1.6032$ for all samples. Thus, Mg doping does not cause any remarkable change in the wurtzite structure of ZnO. This may be due to the comparable ionic radii of Zn^{2+} and Mg^{2+} which made the substitution of Zn^{2+} easy with Mg^{2+} (e.g.[29]-[30]).

Dislocation density is a measure of crystallographic defect or irregularity, within a crystal structure. It is also defined as a topological defect. The movement of a dislocation is impeded by other dislocations present in the sample. Thus, a larger dislocation density implies a larger hardness. The dislocation density δ stands for the magnitude of defects and can be determined by the following relation (e.g. [31]):

$$\delta = 1/D^2 \quad (7)$$

where D is particle size (in nm). In our analysis, the dislocation density was calculated of all samples and the observed data are plotted in Fig.3. From the equation (9), the dislocation density is purely dependent on the crystallite size of the synthesized nanoparticles. The observed values are in between $10^{15}/m^2$ and $1.6.10^{15}/m^2$. From the Fig .3, it clearly shows that the dislocation density varies with respect to the size of the crystal. Low value in δ was noticed for un-doped ZnO. High value in δ was also noticed for the sample $Zn_{0.9}Mg_{0.1}O$. These values are less compared with the published values in literature (e. g [32]). Moreover, the un-doped samples show low value compared to the published values (e. g [33]).

Residual stress is evaluated using the following equation:

$$\sigma = \varepsilon Y \quad (8)$$

where Y is the Young's modulus. For a hexagonal crystal, Young's modulus is given by the following relation (e.g. [34]):

$$Y = \frac{\left[h^2+\frac{(h+2k)^2}{3}+\left(\frac{al}{c}\right)^2\right]^2}{s_{11}\left(h^2+\frac{(h+2k)^2}{3}\right)^2+s_{33}\left(\frac{al}{c}\right)^4+(2s_{13}+s_{44})\left(h^2+\frac{(h+2k)^2}{3}\right)\left(\frac{al}{c}\right)^2} \quad (9)$$

where $S_{11} = 7.858.10^{-12}$, $S_{13} = -2.206.10^{-12}$, $S_{33} = 6.940.10^{-12}$, $S_{44} = 23.57.10^{-12}$ m^2/N respectively [35] are the elastic compliances of ZnO with values. Young's modulus for $Zn_{1-x}Mg_xO$ was calculated and reported in Table 3.

Table.3 Crystallite size, strain, dislocation density and stress of as deposited $Zn_{1-X}Mg_xO$ samples

Samples	Scherrer's method D(nm)	Strain $(\varepsilon \times 10^{-3})$	Dislocation density $\delta.10^{15}m^{-2}$	Young's modulus $Y\ (GPa)$	Stress $\sigma.10^6\ N.m^{-2}$
ZnO	31.30	3.900	1.020	127.26	495.791
$Zn_{0.98}Mg_{0.02}O$	28.07	4.500	1.270	127.26	572.670
$Zn_{0.9}Mg_{0.1}O$	24.64	4.933	1.647	127.26	627.816
$Zn_{0.85}Mg_{0.15}O$	29.02	4.233	1.187	127.26	538.734

3.1.1.3.2. Williamson-Hall method

In the W-H method, the peak width from crystallite size does not follow a $1/\cos\theta$ dependency as in the Scherrer equation but instead varies with $tan\,\theta$. This fundamental difference allows for a separation of reflection broadening when both micro structural causes – small crystallite size and micro strain- occur together. The different approaches presented in the following assume that size and strain broadening are additive components of the total integral breadth of a Bragg peak (e.g. [33]). Addition of the Scherrer equation and $\varepsilon = \beta/4\,tan\,\theta$ results in following equations:

$$\boldsymbol{\beta = \left(\frac{k\lambda}{D\,cos\theta}\right) + 4\varepsilon\,tan\theta} \quad (10)$$

$$\boldsymbol{\beta cos\theta = \left(\frac{k\lambda}{D}\right) + 4\varepsilon\,sin\theta} \quad (11)$$

The above equations are W-H equations. A plot is drawn with $4sin\theta$ along the x-axis and $\beta cos\theta$ along the y-axis for un-doped and Mg doped ZnO nanoparticles as shown in Fig. 5. From the linear fit to the data, the crystalline size D was estimated from the y-intercept, and the strain ε, from the slope of the fit. Eq. (11) represents the uniform deformation model (UDM), where the strain was assumed to be uniform in all crystallographic directions, thus considering the isotropic nature of the crystal, where the material properties are independent of the direction along which they are measured.

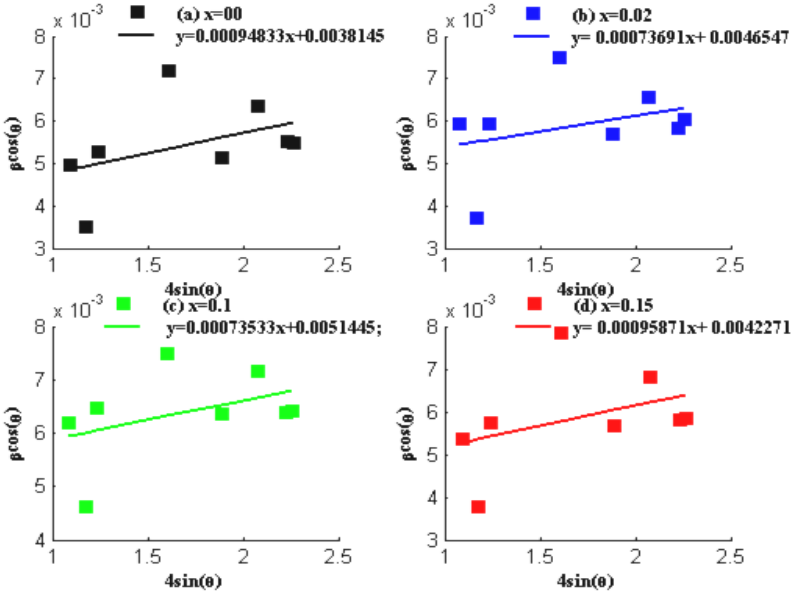

Fig. 5 Plot of $\boldsymbol{\beta cos\theta}$ *versus* $\boldsymbol{4sin\theta}$ of $Zn_{1-X}Mg_xO$ samples

In the Uniform Stress Deformation Model, USDM, a generalized Hooke's law refers to the strain, keeping only the linear proportionality between the stress and strain as given by In the Uniform Stress Deformation Model, USDM, a generalized Hooke's law refers to the strain, keeping only the linear proportionality between the stress and strain as given by $\sigma = \varepsilon Y$. Applying the Hooke's law approximation to Eq. (11) yields:

$$\beta\cos\theta = \left(\frac{k\lambda}{D}\right) + \left(\frac{4\sigma \sin\theta}{Y}\right) \quad \textbf{(12)}$$

Plots were drawn with $(4\ Sin\ \theta/Y)$ on the x-axis and $\beta cos\theta$ on the y-axis, the uniform deformation stress σ can be estimated from the slope of the linear fit and y-intercept gives the crystallite size. The strain ε can be calculated.

There is another model that can be used to determine the energy density of a crystal called the Uniform Deformation Energy Density Model, UDEDM. In Eq. (12), the crystals are assumed to have a homogeneous, isotropic nature. However, in many cases, the assumption of homogeneity and isotropy is not justified. Moreover, the constants of proportionality associated with the stress-strain relation are no longer independent when the strain energy density u is considered. For an elastic system that follows Hooke's law, the energy density u (energy per unit) can be calculated from

$u = (\varepsilon^2 Y)/2$ .Then Eq. (12) can be rewritten according the energy and strain relation:

$$\beta\cos\theta = \left(\frac{k\lambda}{D}\right) + \left(4\ \mathrm{Sin}\theta \left(\frac{2u}{Y}\right)^{1/2}\right) \quad \textbf{(13)}$$

Plot of βcosθ versus $4\ \mathrm{Sin}\theta \left(\frac{2}{Y}\right)^{1/2}$ was done (Fig. 7) and the anisotropic energy density u was estimated from the slope of the linear fit and the crystallite size D from the y-intercept. Previously, we knew that $\sigma = \varepsilon Y$ and $u = (\varepsilon^2 Y)/2$, where the stress σ was calculated as $u = (\sigma^2/2Y)$ .The lattice strain can be calculated.

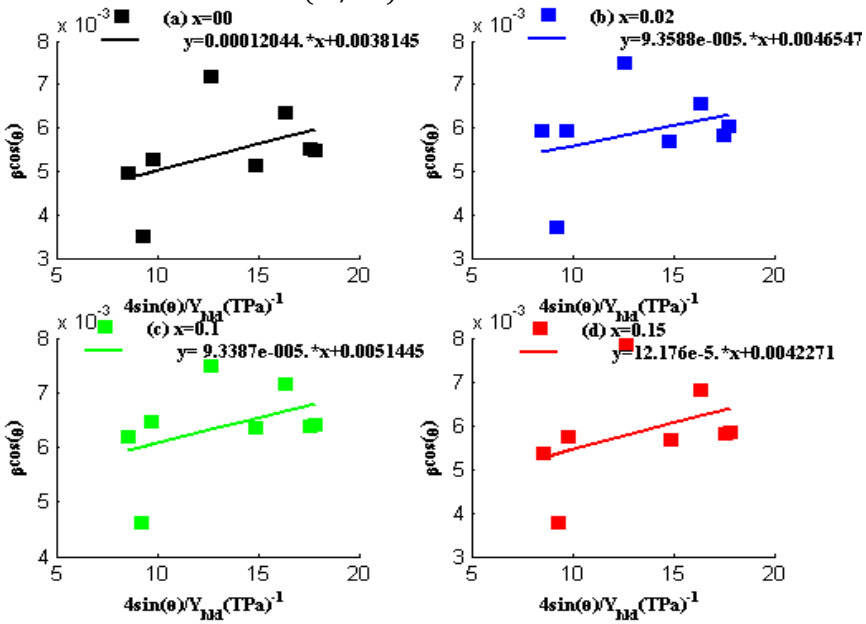

Fig.6 Plot of **βcosθ** *versus* (**4sinθ /Y**) of $Zn_{1-X}Mg_xO$ samples

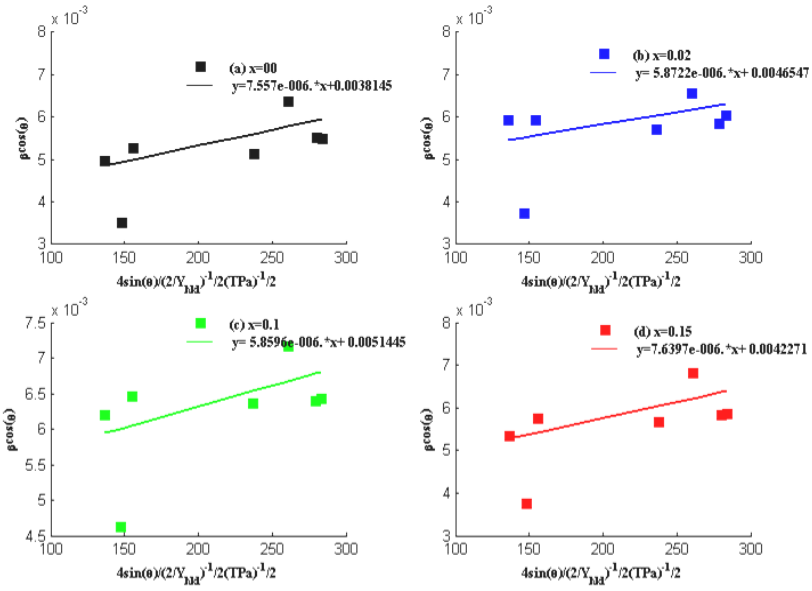

Fig.7 Plot of **βcosθ** versus **4sinθ** $(2/Y)^{1/2}$ of $Zn_{1-X}Mg_xO$ samples

Table.4 The geometric parameters of $Zn_{1-X}Mg_xO$ samples

Samples	UDM		USDM			UDEDM			
	D(nm)	$\varepsilon \times 10^{-3}$	D(nm)	$\sigma(MPa)$	$\varepsilon \times 10^{-3}$	D(nm)	$u(kJ\ m^{-1})$	$\sigma(MPa)$	$\varepsilon \times 10^{-3}$
ZnO	36.35	0.948	36.35	120	0.942	36.35	0.737	57.10	93.78
$Zn_{0.98}Mg_{0.02}O$	29 .80	0.7369	29.78	93 .58	0.735	29.78	0.573	34.48	72.87
$Zn_{0.9}Mg_{0.1}O$	26.95	0.7353	26 .95	93.38	0 .73	26.95	0 .572	34.33	72.71
$Zn_{0.85}Mg_{0.15}O$	32.80	0.9587	32.80	122	0.958	32.80	0.746	58.36	94.20

The results obtained from the Scherrer method, UDM, USDM, UDEDM are summarized in Table 3-4. The values of average crystallite size of the un-doped and Mg doped ZnO nanoparticles obtained from the different models are similar, implying that the inclusion of strain in various forms has a very small effect on the average crystallite size of ZnO-NPs. However, the average crystallite size obtained from the Scherrer formula and the W-H analysis shows the same variation.

In the crystal lattice, the bond length is a key parameter and will change with respect to the process conditions and also the doping element. For hexagonal structure of ZnO, the Zn–O bond length *L* is calculated using the following relations (e.g.[36]).

$$L = \sqrt{\frac{a^2}{3} + \left(\frac{1}{2} - u\right)^2 c^2} \quad \textbf{(14)}$$

Where

$$u = \frac{a^2}{3c^2} + 0.25 \quad \textbf{(15)}$$

Form the relations (14) and (15), it is clearly seen that the bond length is mainly depending on the lattice parameters of the synthesized nanoparticles. Using the lattice parameters values of un-doped and Mg doped ZnO nanoparticles, the bond length is calculated and his variation is reported in Fig.8. This result shows that the bond length is affected by Mg contents. The observed bond length values are lower than the bulk ZnO (1.9778Å) (e.g. [36]).

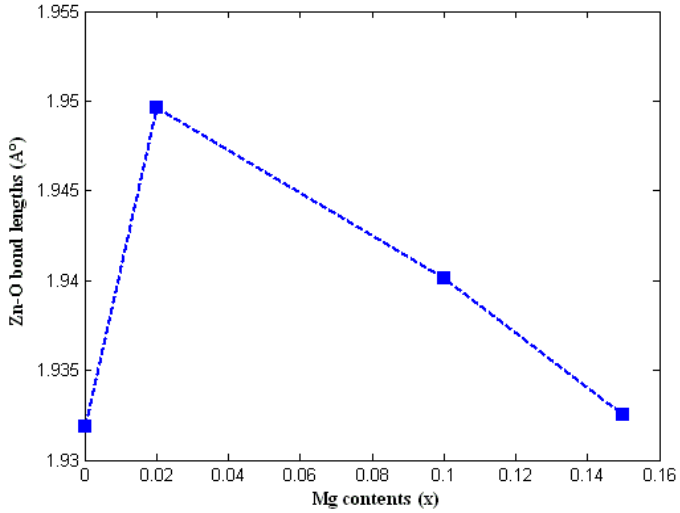

Fig.8 Plot of bond length versus M g contents of $Zn_{1-X}Mg_xO$ samples

3.1.2. Morphological and compositional analysis

Morphology of the samples was studied by scanning electron microscopy. The SEM images of pure and doped ZnO powders at different Mg doping concentrations are shown in Fig.9. The surface of all the samples reveals that the crystallites are of nanometer size. It can be noted that the SEM images of a pressed powders (pellets), makes it difficult to estimate the particle size. However, due to the effect of doping concentration, the surface gets modified and become smoother for higher Mg doping. The images of the surface reveal that the average grain size decreases with increasing Mg contents. This is consistent with the XRD results. The chemical compositions were analyzed by energy dispersive spectroscopy (EDX). Fig.10 shows the EDX spectrum obtained from pure ZnO powders, where only Zn and O are detected, while the presence of magnesium in the ZnO particles (Table 5) is confirmed in all the doped samples.

Table 5 Quantitative results of Mg doped ZnO nanoparticles from EDX analysis

Element	ZnO	$Zn_{0.98}Mg_{0.02}O$	$Zn_{0.9}Mg_{0.1}O$	$Zn_{0.85}Mg_{0.15}O$
O	28.71	10.90	11.68	20.32
Mg	-------	0.56	1.32	4.16
Zn	71.09	88.54	78.00	75.52
Total	100	100	100	100

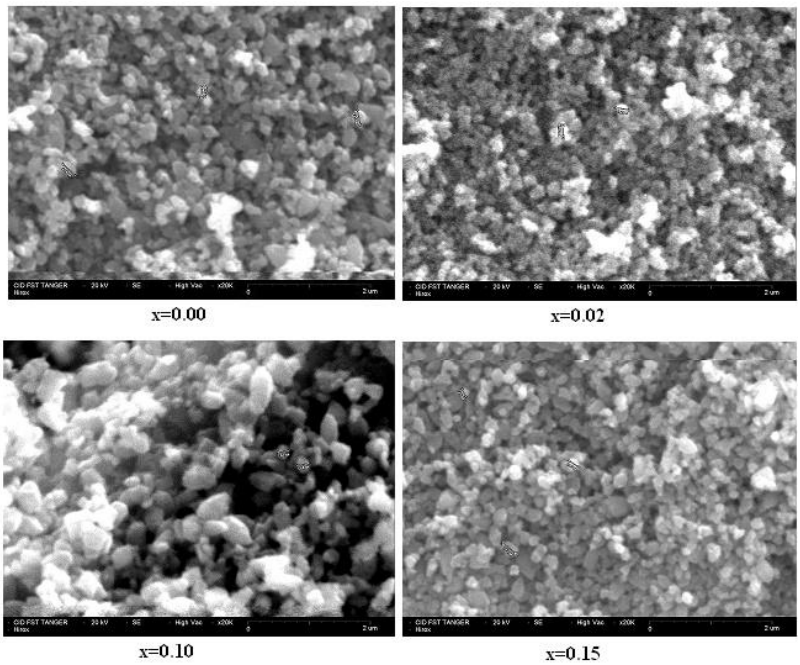

Fig. 9 The SEM images of the $Zn_{1-X}Mg_xO$ samples.

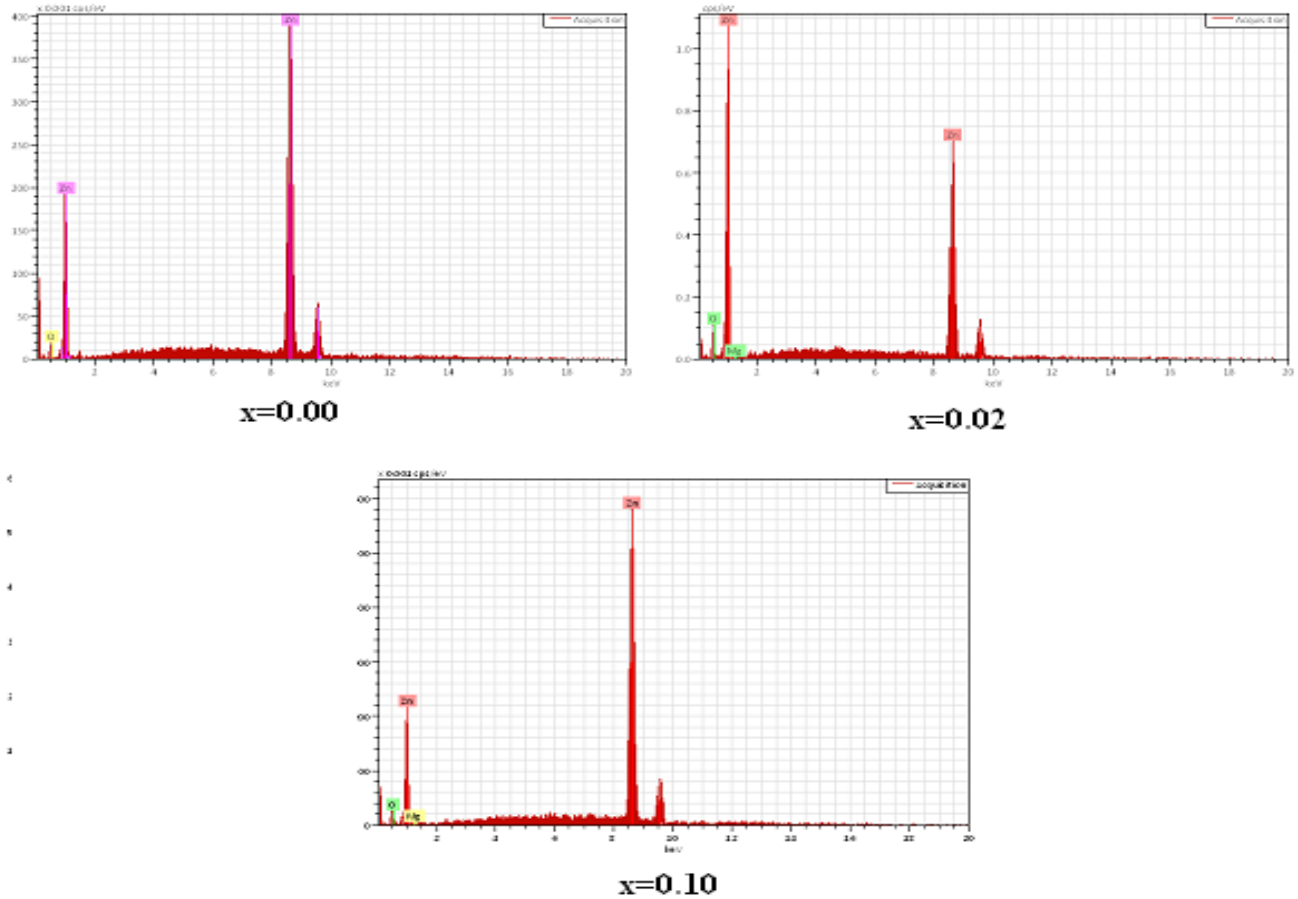

Fig.10 Energy dispersive X-ray (EDX) spectra of $Zn_{1-X}Mg_xO$ samples.

3.1.3. FTIR Analysis

FTIR spectra of $Zn_{1-X}Mg_xO$ with x ranging from 0.00 to 0.15 in the region of 400–4000 cm−1 are shown in Fig.11. The KBr technique has been used to record the spectra. The band located around 600 cm^{-1} can be attributed to the Zn-O stretching mode the ZnO lattice (e.g. [37]). The peaks at 2071 and 2340 cm^{-1}, results from CO_2 and CO (e.g. [38]). The wide peak centred on 3429 cm^{-1} is assigned to O−H stretching vibration due to the bound H_2O on the surface of the sample (e.g. [39]). Additionally, a peak around 1430 cm−1, absent in case of pure ZnO, can be attributed to the Mg−O stretching vibration (e.g. [40]), The FTIR analysis indicates also the presence of Mg element in the Mg doped ZnO samples.

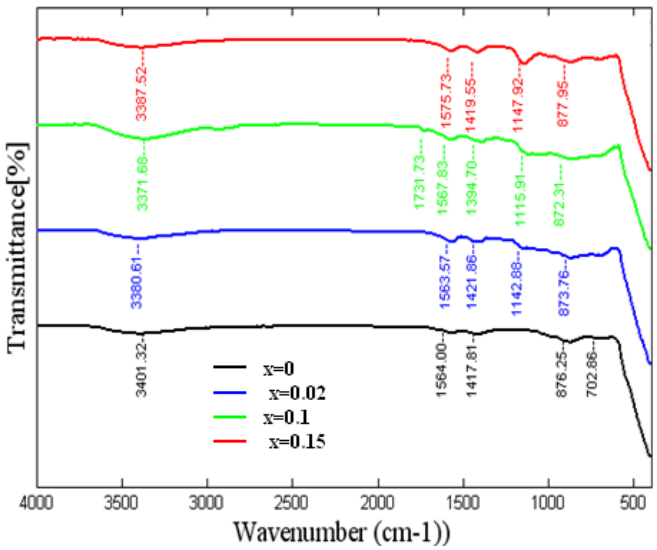

Fig.11 FT-IR spectra of the $Zn_{1-X}Mg_xO$ samples

3.2. Annealing effect

Annealing process is the most important and effective method to control the nanoparticles crystallite size. Consequently, the un-doped ZnO and samples were annealed process at three different temperatures (300°C, 500°C and 800°C). Fig.12 shows the XRD spectra for two samples. The observed indexed peaks in these XRD patterns are fully matched with the corresponding hexagonal wurtzite structure ZnO. With increasing temperature peak height increases and (FWHM) decreases s result diffraction peaks become stronger and sharper, thereby indicating that the crystal quality has been improved and the size of particles become bigger.The values of all the structural parameters estimated from te sherrer's method are summarized in the Table 6.

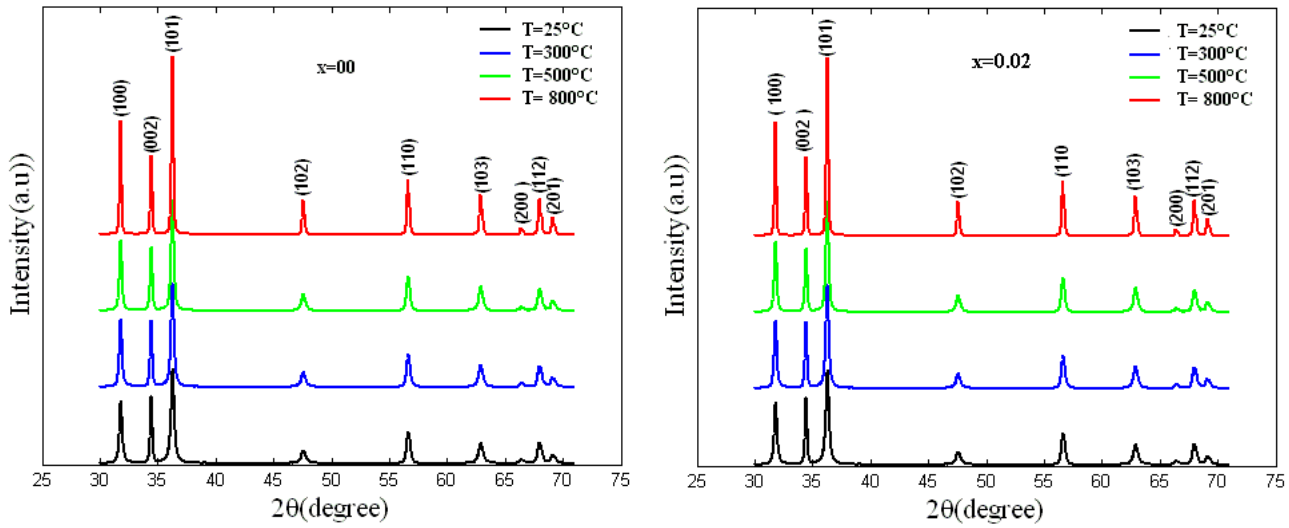

Fig. 12 XRD spectra of the un-doped and Mg doped ZnO nanoparticles for different Temperatures.

Table6. Structural parameters of $Zn_{1-x}Mg_xO$ at different Temperatures.

Compound $Zn_{1-x}Mg_xO$		2θ value(°)	⟨hkl⟩	d_{hkl}(Å)	Strain (ε $\times 10^{-3}$)	Lattice parametr (A°)	Particle Size D_{hkl} (nm)	Average Size (nm)	$TC_{(hkl)}$
x = 0.00	300	31.8134	⟨100⟩	2.111	3.4	a = 3.2454	*30.60*	*32.34*	*1.1438*
		34.44646	⟨002⟩	2.281	3.2	c = 5.2031	*39.15*		***1.516***
		36.29178	⟨101⟩	2.399	3.0	c/a = 1.6027	*27.23*		*0.9885*
	500	31.81459	⟨100⟩	2.111	3.7	a = 3.2453	*32.72*	*34.73*	*1.1384*
		34.45665	⟨002⟩	2.281	3.1	c = 5.2016	*41.78*		***1.3911***
		36.2926	⟨101⟩	2.399	3.9	c/a = 1.6023	*29.69*		*1.0204*
	800	31.80369	⟨100⟩	2.111	2.7	a = 3.2463	*45.77*	*43.28*	*1.2189*
		34.4619	⟨002⟩	2.281	2.7	c = 5.2008	*42.82*		***1.1309***
		36.29015	⟨101⟩	2.399	2.7	c/a = 1.6020	*41.23*		*1.0860*

		31.79703	⟨100⟩	2.110	3.4	a = 3.2470	*33.10*		*1.2493*
	300	34.44948	⟨002⟩	2.281	3.2	c = 5.2026	*32.02*	*31.72*	***1.2331***
		36.28198	⟨101⟩	2.398	3.3	c/a = 1.6018	*30.04*		*1.1452*
x	500	31.7876	⟨100⟩	2.110	3.7	a = 3.2479	*33.57*		*1.1483*
= 0.02		34.43952	⟨002⟩	2.280	3.4	c = 5.2041	*34.75*	*33.00*	***1.2189***
		36.27009	⟨101⟩	2.398	3.7	c/a = 1.6023	*30.68*		*1.0385*
	800	31.79009	⟨100⟩	2.110	2.7	a = 3.2470	*42.45*		*1.1950*
		34.44974	⟨002⟩	2.281	2.7	c = 5.2026	*40.50*	*40.40*	***1.2061***
		36.27688	⟨101⟩	2.398	2.6	c/a = 1.6019	*38.25*		*1.0786*

The variation of crystallite size with annealing temperature is shown in Fig. 13. It is observed that the crystallite size increases with increasing temperature. The larger size values indicate better crystallization of the nanoparticles. As shown in Fig. 13, dislocation densities exhibits a decreasing trend with increasing temperature

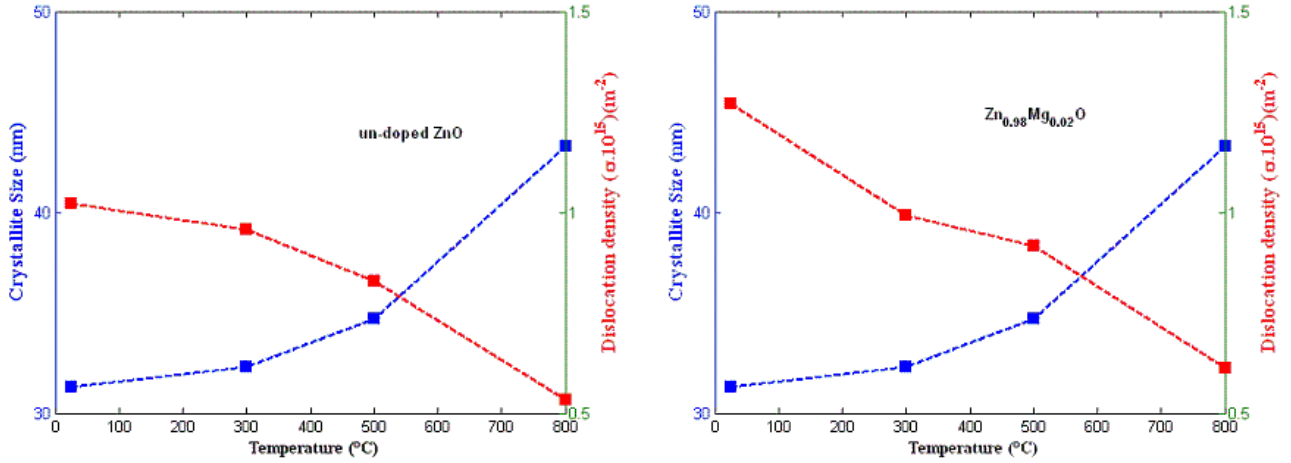

Fig.13 Crystallite size and dislocation density values of the $Zn_{1-x}Mg_xO$ dependence on Temperatures.

.

IV. CONCLUSIONS

Un-doped and Mg doped ZnO nanoparticles were synthesized by a simple sol-gel method. The results of the XRD showed that the average particle size varies with the Mg contents and thermal annealing. The average values of crystallite size obtained from UDM, UDSM, and UDEDM are almost similar, which indicate the inclusion of strain in various forms of W–H analysis has a very small effect on the average crystallite size. The SEM coupled with EDX measurement indicates the incorporation of Mg in the samples. Furthermore, the FTIR showed an absorption vibration band related to Mg-O.

ACKNOWLEDGMENTS

The authors gratefully acknowledge the responsible of National Center for Nuclear Science and Technology and Faculty of Science and Technology of Tanger for the experimental characterization.

REFERENCES

[1] C. Jagadish, S. J. Pearton, "*Zinc oxide bulk, Thin films and Nanostructures*", Amsterdam, Elsevier, 2006.

[2] Z. L. Wang, "Zinc oxide nanostructures: growth properties and applications," *J.Phys : Condens. Matter.*, vol. 16, pp. R829-R858, 2004.

[3] A. K. Radzimska and T. Jesionowski, "Zinc oxide From synthesis to Applications: A review," *Materials*, vol.7, pp. 2833-2881, 2014.

[4] Ü. Özgür, Ya I. Alivov, C. Liu, A. Teke, M. A. Reshchikov, S. Dogan, V. Avrutin,S.-J.Cho, and H.Morko ,"A comprehensive review of ZnO materials and devices", *Journal of Applied Physics* ,vol.98, pp.041301-041404, 2005.

[5] S. barnah, Samir K.Pal and J. Dutta, "Nanostructured Zinc Oxide for water treatment", *Nanoscience&Nanotechnology-Asia*, vol.2, pp. 90-102, 2012.

[6] Z. Ling, C. Leoch, R. Freer, "Heterojunction gas sensors for environmental NO2 and CO2 monitoring," *J. Eur. Ceram. Soc.*, vol. 21, pp. 1977–1980, 2001.

[7] C. Y. Hsu, T. F. Ko, Y.M. Huang, "Influence of ZnO buffer layer on AZO film properties by radio frequency magnetron sputtering",*J. Eur. Ceram.Soc.*,vol.28, 3065-3070, 2008.

[8] C.C. Vàzquez, R. Bernal, S.E. Burrnel-Ibarra, h. Crijalva-Monteverde, M.Barboza-Flores, "Thermoluminescence properties of new ZnO nanophosphors exposed to beta irradiation", *Optical Materials*, vol. 27, pp.1235-1239, 2005.

[9] A. K. Srivastava Chakraborty, S.Chandra, "Induced thermoluminescence of X-ray irradiated nanostructured zinc oxide", *Optical Materials*, vol. 32, pp. 410-413, 2009.

[10] Y.M. Kim, M. Yoon, I.W. Park, Y.J. Park, J. H. Lyou, "Synthesis and magnetic properties of Zn12xMnxO films prepared by the sol– gel method", *Solid State Communications* ,vol.129 ,pp.175–178, 2004.

[11] J. El Ghoul, C. Barthou, L. El Mir, "Synthesis by sol–gel process, structural and optical properties of nanoparticles of zinc oxide doped vanadium", *Superlattices and Microstructures*, vol.51,pp. 942–951, 2012.

[12] J. El Ghoul, C. Barthou, L. El Mir, "Synthesis, structural and optical properties of nanocrystalline vanadium doped zinc oxide aerogel", *Physica E*,vol. 44,pp. 1910–1915, 2012.

[13] L. El Mir, J. El Ghoul, S. Alaya, M. Ben Salem, C. Barthou, H. J. von Bardeleben, "Synthesis and luminescence properties of vanadium- doped man-sized zinc oxide aeroge," *Physica B: Condensed Matter*. , vol. 403, pp.1770–1774, 2008.

[14] J. El Ghoul, C. Barthou, M. Saadoun and L. El Mir, "Synthesis and optical characterization of SiO2/Zn2SiO4:Mn nanocomposite," *Physica B: condensed Matter.*, vol. 405,pp, 597–601, 2010.

[15] L. El Mir, Z. Ben Ayadi, M. Saadoun, K. Djessas, H.J. von Bardeleben, S. Alaya, " Preparation and characterization of n-type conductive (Al, Co) co-doped ZnO thin films deposited by sputtering from aerogel nanopowders," *J. Appl. Surf. Sci.*, vol.254, pp. 570-573, 2007.

[16] D. Karmakar, S.K. Mandal, R.M. Kadam, P.L. Paulose, A.K. Rajarajan, T.K. Nath, A.K. Das, I. Dasgupta, G.P. Das, "Ferromagnetism in Fe-doped ZnO nanocrystals: Experiment and theory", *J. Phys. Rev. B*, vol.75, pp. 144404-1444028, 2007.

[17] A. K. Zak, W.H. Abd. Majid, M.E. Abrishami, R. Yousefi, R. Parvizi, "Synthesis, magnetic properties and X-ray analysis of Zn 0.97 X 0.03 O nanoparticles (X= Mn, Ni, and Co) using Scherrer and size–strain plot methods", *J. Solid State Sci.*, vol.14, pp.488-494, 2012.

[18] Chen CC, Liu P, Lu CH, "Synthesis and characterization of nanosized ZnO powders by direct precipitation method", *Chem. Eng. J*. 1444, 509-513 , 2008.

[19] Ristiac,M., Musiac,S., Ivanda,M., Popovia,S. : Sol gel synthesis and characterization of nanocrystalline ZnO powders, *J.Alloys .Compd*, 397, L1 – L4 , 2007

[20] S.Suwanboon and P.Amornpitoksuk, Preparation of Mg-doped ZnO nanoparticles by mechanical milling and their optical properties, *Procedia Engineering*, vol.32, pp.821-826, 2012.

[21] M. Arshad, M.M. Ansari, A. Ahmed, P. Tripathi, S. Ashraf, A. Naqvi and A. Azam, "Band gap engineering and enhanced photoluminescence of Mg doped ZnO nanoparticles synthesized by wet chemical route," *J. Luminescence*, vol. 161, pp. 275 - 280, 2015.

[22] C.S. Barret, T.B. Massalski, "*Structure of Metals: Crystallographic Methods, Principles and Data*", Pergamon Press: Oxford, UK, 1980, p. 204.

[23] A. L. Patterson, "*The Scherrer Formula for X-Ray Particle Size Determination*", Phys. Rev., vol. 56, pp.978–982, 1939.

[24] C. S. Prajapati and P. P. Sahay, "Growth, structure and optical characterization of Al-doped ZnO nanoparticle thin films", *Cryst. Res. Technol*., vol. 46, pp.1086- 1092, 2011.

[25] C. Prajapati and P. Sahay, "Influence of In doping on the structural, optical and acetone sensing properties of ZnO nanoparticulate thin films," *Mater. Sci. Semicond.* Process. , vol.6, pp. 200-210, 2012.

[26] H. Chen, J. Ding, and S. Ma, "Structural and optical properties of ZnO:Mg thin films grown under different oxygen partial pressures", *Physica. E*, vol.42, pp. 1487–1491, 2010.

[27] H.P. Klug, L.E. Alexander, "*X-Ray Diffraction Procedures for Polycrystalline and Amorphous Materials*", (Wiley Publishing, 1974).

[28] B.D. Cullity, S.R. Stock, "*Elements of X-ray diffraction*", 3rd edn. Prentice Hall, New Jersey (2001).

[29] H. Zhuang, J. Wang, H. Liu, J. Li, and P. Xu, " Structural and Optical Properties of ZnO Nanowires Doped with Magnesium", *Acta Phys. Polonica A*.vol.119, pp. 819-823, 2011.

[30] J. Singh, M.S.L. Hudson, S.K. Pandey, R.S. Tiwari, and O.N. Srivastava, "Structural and Hydrogenation Studies of ZnO and Mg Doped ZnO Nanowires", *Int. J. Hydrogen.Energy*.,vol.37, pp.3748-3754, 2012.

[31] M. Saleem, L. Fang, H.B. Ruan, F. Wu, F, Q.L. Huang, C.L. Xu, C.Y. Kong, "Effect of zinc acetate concentration on the structural and optical properties of ZnO thin films deposited by sol-gel method", *Intl. J. Phy. Sci*., vol.7, pp. 2971–2979, 2012.

[32] A.J. Perry, "The state of residual-stress in Tin films made by physical vapor-deposition methods - the stateof-the-art," *J. Vac. Sci. Technol*., vol. 8, pp. 1351 - 1358, 1990.

[33] M. Mazhdi and P. Hossein Khani, "Structural characterization of ZnO and ZnO:Mn nanoparticles prepared by reverse micelle method," *Int. J. Nano. Dimens.* , vol. 2, pp. 233 - 240, 2012.

[34] B.E.Warren, B.L. Averbach, "The effect of cold-work distorsion on X- ray pattems," *J. Appl. Phys*., vol. 21, pp. 595 595–599, 1950.

[35] J.F. Nye, "*Physical Properties of Crystals: Their Representation by Tensor and Matrices*", Oxford, New York, pp.329, 1985.

[36] S. Ilican, Y. Caglar and M. Caglar, "Preparation and characterization of ZnO thin films deposited by sol-gel spin coating method", *J. Optoelectron. Adv. Mater.*, vol.10, pp. 2578 - 2583, 2008.

[37] A.E. Jimenez-Gonzalez, J.A.S. Urueta, R. Suarez-Parra, "Optical and electrical characteristics of aluminum-doped ZnO thin films prepared by sol-gel technique," *J. Cryst .Growth,* vol. 192, pp.430–438, 1998.

[38] M. Kacurakova, R.H. Wilson, "Developments in mid-infrared FT-IR spectroscopy of selected carbohydrates", *Carbohyd. Polym.* , vol. 44, 291-303, 2001.

[39] M. Schiek, K. Al-Shamery, M. Kunat, F. Traeger, C. Woll, "Water adsorption on the hydroxylated H-(1 × 1) O-ZnO(000$\bar{1}$) surface", *Phys. Chem. Chem. Phys.*,vol.8, pp 1505-1512, 2006.

[40] T. Lopez, I. Garcia-Cruz, R. Gomez, "Synthesis of Magnesium Oxide by the Sol-Gel. Method: Effect of pH on the Surface Hydrolixation", *J. Catalysis*, vol.127, pp. 75-85, 1991.

[41] G.H, Guang-hui, X.P. Zhao, J. Li, "Structure and optical properties of Mg*x*Zn1−*x*O nanoparticles prepared by sol–gel method", *Optical Materials*, vol. 27, pp.1-5, 2004.

